Available online at www.sciencedirect.com
SCIENCE DIRECT®
International Journal of Solids and Structures 42 (2005) 4372–4392
INTERNATIONAL JOURNAL OF SOLIDS and STRUCTURES
www.elsevier.com/locate/ijsolstr

Micromechanical analysis of lattice blocks

Jacob Aboudi [a,*], Rivka Gilat [b]

[a] *Faculty of Engineering, Department of Solid Mechanics, Tel Aviv University, Ramat Aviv 69978, Israel*
[b] *Faculty of Engineering, The College JAS Ariel, Ariel 44837, Israel*

Received 24 October 2004; received in revised form 13 January 2005
Available online 16 February 2005

Abstract

Multiphase lattice blocks with periodic structure are analyzed by a continuum-based micromechanical approach. As a result, effective stiffness tensors, global initial yield surfaces, global damage thresholds, effective inelastic stress–strain responses and critical yielding temperatures of lattice blocks are established. Applications are given for various types of elastic and inelastic lattice blocks made of an aluminum alloy. Furthermore, a lattice block with negative effective Poisson's ratios is considered, and two types of two-phase lattice blocks that are capable to produce negative effective coefficients of thermal expansion are presented.

Keywords: Micromechanics; Homogenization; Yield surface; Negative Poisson's ratio; Re-entrant configuration; High fidelity generalized method of cells (HFGMC)

1. Introduction

Cellular materials (e.g. metallic foams and bones) are composed of random distribution of open or closed cells, see Gibson and Ashby (1997) for a detailed discussion. Lattice blocks, on the other hand, are periodic structures that are based on a repeating unit cell, see Evans et al. (2001) where the advantages, benefits, design and manufacturing of these structures are discussed, together with comparisons of their capabilities with cellular materials. In particular, lattice block have been shown to provide very high stiffness and strength with only a fraction of the weight of the parent material. Emerging applications of lattice block structure range from ultra-light weight multi-functional structures to automobile, aerospace components, furniture and sporting goods, Zhou et al. (2004).

* Corresponding author. Tel.: +972 36408131; fax: +972 36407617.
E-mail address: aboudi@eng.tau.ac.il (J. Aboudi).

0020-7683/$ - see front matter © 2005 Elsevier Ltd. All rights reserved.
doi:10.1016/j.ijsolstr.2005.01.008

Lattice blocks have been investigated by Wallach and Gibson (2001), Deshpande et al. (2001), Chiras et al. (2002), and Zhou et al. (2004). Sandwich plates with truss cores are also periodic structures that were analyzed by Wicks and Hutchinson (2001), Hutchinson et al. (2003), and Wicks and Hutchinson (2004). In a recent article, Wang and McDowell (2005) derived the initial yield surfaces of various types of periodic metal honeycombs.

In the previous investigations the periodic structures have been analyzed by a detailed study of the behavior of the beam members which form the basic elements of the lattice block. Alternatively, in the present investigation we offer the use of a micromechanical approach, that has been previously developed for the prediction of the behavior of multi-phase periodic composites, for analyzing periodic lattice blocks. In the framework of this continuum mechanics-based approach the repeating unit cell, which forms the building block of the three-dimensional lattice material, is divided into several parallelepiped subcells. Some of these subcells are appropriately filled by the material while leaving the other subcells empty. In the micromechanical analysis of the resulting discretized repeating unit cell, the material within a filled subcell is modeled by the standard multi-axial constitutive law that governs its behavior (the generalized Hooke's law for elastic anisotropic materials, inelastic constitutive relations for elastoplastic or viscoplastic materials, etc.).

The specific micromechanical analysis that is employed in this paper to study the response of lattice blocks is referred to as high fidelity generalized method of cells (HFGMC) which is based on the homogenization technique of periodic composites. In the two-dimensional case, HFGMC has been established and verified by Aboudi et al. (2001, 2003) for thermoelastic and thermoinelastic composites, respectively, and implemented by Bednarcyk et al. (2004) in the case of inelastic matrix with fiber-matrix debonding. The three-dimensional version of HFGMC has been presented and verified by Aboudi (2001) where it was implemented to study the behavior of electro-magneto-thermo-elastic multi-phase composites. This micromechanical theory has been recently reviewed by Aboudi (2004). In addition to the effective moduli and inelastic response prediction of the periodic lattice blocks, HFGMC is employed for the generation of their initial yield surfaces, yield temperatures and damage envelopes. It should be noted that the HFGMC has been implemented into the recently developed micromechanics analysis code MAC/GMC by NASA Glenn Research Center, which has many user friendly features and significant flexibility, see Bednarcyk and Arnold (2002) for the most recent version of its user guides.

The present paper is organized as follows. A brief summary of the three-dimensional HFGMC is given, and closed-form expressions for the effective stiffness and thermal stress tensors of the multi-phase lattice block in terms of its mechanical and thermal concentration tensors (which relate the applied external strain and temperature to the local ones) are provided. Furthermore, in terms of these tensors, expressions are derived for the establishment of the initial yield surfaces, damage thresholds and the critical temperature for yielding. The present approach has been applied on six types of lattice blocks made of an aluminum alloy, including the configurations of Zhou et al. (2004) and Chiras et al. (2002), for the prediction of the effective stiffness tensors. Next, the micromechanically established elastoplastic response of the lattice blocks is presented by taking into account the inelastic behavior of the aluminum material. It turns out that for certain lattice block configurations and loading directions, the elastoplastic stress–strain relation can be computed for any loading amplitude. In other circumstances, on the other hand, the lattice block loses, at certain loading directions and amplitudes, its stiffness and stability such that the multiplication of the increments of global stress and strain is negative. This type of response resembles the well known behavior that is exhibited by the relation between the load and deflection of nonlinear structures (Majid, 1972). Initial yield surfaces are presented for the considered types of lattice blocks, and the critical temperatures at which yielding occurs are computed.

Foam structures with negative Poisson's ratio have been produced by Lakes (1987) from conventional open cell polymer foams by constructing a re-entrant type of network. Most of the approaches for the modeling of materials with negative Poisson's ratio are based on the analysis of reticulated structures whose

elements are made of beams. Almgren (1985), for example, analyzed a structure with a negative Poisson's ratio that consists of rods, hinges and springs. Similarly, Choi and Lakes (1995) investigated materials with negative Poisson's ratios by analyzing spatial struts and curved beams. In the present paper, following our approach for the micromechanical modeling of periodic structures, a lattice block with three orthogonal re-entrant configurations that is capable to produce negative effective Poisson's ratios is presented and analyzed.

By considering certain types of microstructures composed of at least two materials possessing positive thermal expansion coefficients, it is possible to generate effective negative coefficients of thermal expansion. For a two-dimensional array of phases this capability has been presented by Kalamkarov and Kolpakov (1997). Here, we propose two types of two-phase periodic lattice blocks which are capable to generate negative effective coefficients of thermal expansion.

2. Micromechanical analysis

The HFGMC micromechanical model is employed herein to predict the effective thermoinelastic properties of the lattice blocks. This theory has been fully described by Aboudi (2001) in the case of linear electro-magneto-thermo-elastic materials. Thus, thermoelastic phases can by obtained as a special case. The inclusion of inelastic of the phases follow the analysis that has been presented by Aboudi et al. (2003) in the two-dimensional case of continuous fibers. In the present paper, this micromechanical model is briefly outlined in the following.

This model is based on a homogenization technique for composites with periodic microstructure as shown in Fig. 1(a) in terms of the global coordinates (x_1, x_2, x_3). The parallelepiped repeating unit cell, Fig. 1(b), defined with respect to local coordinates (y_1, y_2, y_3), of such a composite is divided into N_α, N_β

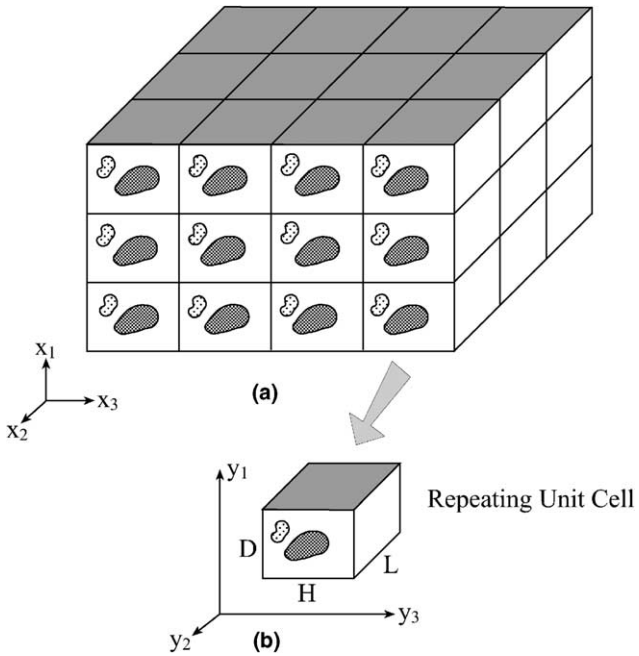

Fig. 1. (a) A multi-phase composite with periodic microstructures defined with respect to global coordinates (x_1, x_2, x_3). (b) The repeating unit cell is represented with respect to local coordinates (y_1, y_2, y_3).

and N_γ subcells in the y_1, y_2 and y_3 directions, respectively. Each subcell is labeled by the indices $(\alpha\beta\gamma)$ with $\alpha = 1,\ldots,N_\alpha$, $\beta = 1,\ldots,N_\beta$ and $\gamma = 1,\ldots,N_\gamma$, and may contain a distinct homogeneous material. The dimensions of subcell $(\alpha\beta\gamma)$ in the y_1, y_2 and y_3 directions are denoted by d_α, h_β and l_γ, respectively. A local coordinate system $(\bar{y}_1^{(\alpha)}, \bar{y}_2^{(\beta)}, \bar{y}_3^{(\gamma)})$ is introduced in each subcell whose origin is located at its center.

The local (subcell) constitutive equation of the material which, in general, is assumed to be thermoinelastic is given by

$$\boldsymbol{\sigma}^{(\alpha\beta\gamma)} = \mathbf{C}^{(\alpha\beta\gamma)}\left(\boldsymbol{\epsilon}^{(\alpha\beta\gamma)} - \boldsymbol{\epsilon}^{\mathrm{I}(\alpha\beta\gamma)}\right) - \boldsymbol{\Gamma}^{(\alpha\beta\gamma)}\Delta T \tag{1}$$

where $\boldsymbol{\sigma}^{(\alpha\beta\gamma)}$, $\boldsymbol{\epsilon}^{(\alpha\beta\gamma)}$, $\boldsymbol{\epsilon}^{\mathrm{I}(\alpha\beta\gamma)}$ and $\boldsymbol{\Gamma}^{(\alpha\beta\gamma)}$ are the stress, total strain, inelastic strain and thermal stress tensors, respectively, in subcell $(\alpha\beta\gamma)$. In Eq. (1), $\mathbf{C}^{(\alpha\beta\gamma)}$ is the stiffness tensor of the material in the subcell $(\alpha\beta\gamma)$, and ΔT denotes the temperature deviation from a reference temperature. The inelastic strain $\boldsymbol{\epsilon}^{\mathrm{I}(\alpha\beta\gamma)}$ is governed either by the Prandtl–Reuss equations of the classical plasticity or by an appropriate viscoplastic flow rule.

The basic assumption in HFGMC is that the displacement vector $\mathbf{u}^{(\alpha\beta\gamma)}$ in each subcell is expanded into quadratic forms in terms of its local coordinates $(\bar{y}_1^{(\alpha)}, \bar{y}_2^{(\beta)}, \bar{y}_3^{(\gamma)})$ as follows:

$$\begin{aligned}\mathbf{u}^{(\alpha\beta\gamma)} = {} & \bar{\boldsymbol{\epsilon}}\,\mathbf{x} + \mathbf{W}_{(000)}^{(\alpha\beta\gamma)} + \bar{y}_1^{(\alpha)}\mathbf{W}_{(100)}^{(\alpha\beta\gamma)} + \bar{y}_2^{(\beta)}\mathbf{W}_{(010)}^{(\alpha\beta\gamma)} + \bar{y}_3^{(\gamma)}\mathbf{W}_{(001)}^{(\alpha\beta\gamma)} + \frac{1}{2}\left(3\bar{y}_1^{(\alpha)2} - \frac{d_\alpha^2}{4}\right)\mathbf{W}_{(200)}^{(\alpha\beta\gamma)} \\ & + \frac{1}{2}\left(3\bar{y}_2^{(\beta)2} - \frac{h_\beta^2}{4}\right)\mathbf{W}_{(020)}^{(\alpha\beta\gamma)} + \frac{1}{2}\left(3\bar{y}_3^{(\gamma)2} - \frac{l_\gamma^2}{4}\right)\mathbf{W}_{(002)}^{(\alpha\beta\gamma)}\end{aligned} \tag{2}$$

where $\bar{\boldsymbol{\epsilon}}$ is the applied (external) average strain, and the unknown terms $\mathbf{W}_{(lmn)}^{(\alpha\beta\gamma)}$, must be determined from the fulfillment of the equilibrium conditions, the periodic boundary conditions, and the interfacial continuity conditions of displacements and tractions between subcells. The periodic boundary conditions ensure that the displacements and tractions at opposite surfaces of the repeating unit cell are identical, see Aboudi (2001) for more details. A principal ingredient in the present micromechanical analysis is that all these conditions are imposed in the average (integral) sense.

As a result of the imposition of these conditions, a linear system of algebraic equations is obtained which can be represented in the following form:

$$\mathbf{K}\mathbf{U} = \mathbf{f} + \mathbf{g} \tag{3}$$

where the matrix $\mathbf{K}$ contains information on the geometry and thermomechanical properties of the materials within the individual subcells $(\alpha\beta\gamma)$, and the displacement vector $\mathbf{U}$ contains the unknown displacement coefficient $\mathbf{W}_{(lmn)}^{(\alpha\beta\gamma)}$ which appear on the right-hand side of Eq. (1). The mechanical vector $\mathbf{f}$ contains information on the applied average strains $\bar{\boldsymbol{\epsilon}}$ and the imposed temperature deviation ΔT. The inelastic force vector $\mathbf{g}$ appearing on the right-hand side of Eq. (3) contains the inelastic effects given in terms of the integrals of the inelastic strain distributions. These integrals depend implicitly on the elements of the displacement coefficient vector $\mathbf{U}$, requiring an incremental procedure of Eq. (3) at each point along the loading path, see Aboudi et al. (2003) for more details.

The solution of Eq. (3) enables the establishment of the following localization relation which expresses the average strain $\bar{\boldsymbol{\epsilon}}^{(\alpha\beta\gamma)}$ in the subcell $(\alpha\beta\gamma)$ to the externally applied average strain $\bar{\boldsymbol{\epsilon}}$ in the form (Aboudi, 2004):

$$\bar{\boldsymbol{\epsilon}}^{(\alpha\beta\gamma)} = \mathbf{A}^{(\alpha\beta\gamma)}\bar{\boldsymbol{\epsilon}} + \mathbf{A}^{\mathrm{th}(\alpha\beta\gamma)}\Delta T + \mathbf{D}^{\mathrm{I}(\alpha\beta\gamma)} \tag{4}$$

where $\mathbf{A}^{(\alpha\beta\gamma)}$ and $\mathbf{A}^{\mathrm{th}(\alpha\beta\gamma)}$ are the mechanical and thermal strain concentration tensors, respectively, of the subcell $(\alpha\beta\gamma)$, and $\mathbf{D}^{\mathrm{I}(\alpha\beta\gamma)}$ is a vector that involves the current inelastic effects in the subcell.

The final form of the effective constitutive law of the multi-phase thermo-inelastic composite, which relates the average stress $\bar{\boldsymbol{\sigma}}$ and strain $\bar{\boldsymbol{\epsilon}}$, is established as follows:

$$\bar{\boldsymbol{\sigma}} = \mathbf{C}^{*}\bar{\boldsymbol{\epsilon}} - (\boldsymbol{\Gamma}^{*}\Delta T + \bar{\boldsymbol{\sigma}}^{\mathrm{I}}) \tag{5}$$

In this equation $\mathbf{C}^*$ is the effective stiffness tensor and $\boldsymbol{\Gamma}^*$ is the effective thermal stress tensor of the composite, and $\bar{\boldsymbol{\sigma}}^{\mathrm{I}}$ is the global inelastic stress tensor. All these global quantities can be expressed in a closed-form manner in terms of the mechanical and thermal concentration tensors which appear in Eq. (4) together with the inelastic term $\mathbf{D}^{\mathrm{I}(\alpha\beta\gamma)}$, see Aboudi (2004) for more details. In particular,

$$\mathbf{C}^{*} = \frac{1}{DHL} \sum_{(\alpha\beta\gamma)\ \text{of filled subcells}} d_{\alpha}h_{\beta}l_{\gamma}\mathbf{C}^{(\alpha\beta\gamma)}\mathbf{A}^{(\alpha\beta\gamma)} \tag{6}$$

and

$$\boldsymbol{\Gamma}^{*} = \frac{-1}{DHL} \sum_{(\alpha\beta\gamma)\ \text{of filled subcells}} d_{\alpha}h_{\beta}l_{\gamma}[\mathbf{C}^{(\alpha\beta\gamma)}\mathbf{A}^{\mathrm{th}(\alpha\beta\gamma)} - \boldsymbol{\Gamma}^{(\alpha\beta\gamma)}] \tag{7}$$

It should be emphasized that lattice blocks are necessarily three-dimensional and numerous subcells might be needed to analyze the repeating unit cell. Consequently, the number of equations can be large which makes the memory and computer time requirements formidable. Hence a special strategy has been adopted according to which whenever a subcell is found to be empty with no material inside it, this subcell is skipped (rather than being incorporated in the analysis by assuming that its material constants are vanishingly small). In this way unfilled subcells in the repeating unit cell do not participate in its analysis. As a result, the number of equations is considerably reduced since only filled subcell participate in the analysis of the lattice block. However, for a filled subcell neighboring an empty subcell, traction-free boundary conditions must be imposed at its corresponding surface. The significant saving in the reduction of the number of equations can be illustrated in the case of a lattice block, which will be considered in the sequel, in which the repeating unit cell consists of $N_\alpha = N_\beta = N_\gamma = 34$ subcells. Here the number of subcells is 39,304, but the number of filled subcells is 4216 only. This necessitates the solution of 75,888 equations instead of 707,472 (since there are 18 unknowns in each filled subcell).

In order to generate the initial yield envelopes and the temperature at which yielding initiates, the mechanical and thermal stress concentration tensors must be established. By combining Eqs. (1), (4) and (5), in the absence of inelastic effects, one obtains after some manipulations that the average stress in a subcell is given in terms of the externally applied average strain and temperature by

$$\bar{\boldsymbol{\sigma}}^{(\alpha\beta\gamma)} = \mathbf{C}^{(\alpha\beta\gamma)}\mathbf{A}^{(\alpha\beta\gamma)}\bar{\boldsymbol{\epsilon}} + \mathbf{E}^{\mathrm{th}(\alpha\beta\gamma)}\Delta T \tag{8}$$

where

$$\mathbf{E}^{\mathrm{th}(\alpha\beta\gamma)} = \mathbf{C}^{(\alpha\beta\gamma)}\mathbf{A}^{\mathrm{th}(\alpha\beta\gamma)} - \boldsymbol{\Gamma}^{(\alpha\beta\gamma)}$$

In terms of the externally applied stress and temperature, on the other hand, the average local stress is given by

$$\bar{\boldsymbol{\sigma}}^{(\alpha\beta\gamma)} = \mathbf{B}^{(\alpha\beta\gamma)}\bar{\boldsymbol{\sigma}} + \mathbf{B}^{\mathrm{th}(\alpha\beta\gamma)}\Delta T \tag{9}$$

where

$$\mathbf{B}^{(\alpha\beta\gamma)} = \mathbf{C}^{(\alpha\beta\gamma)}\mathbf{A}^{(\alpha\beta\gamma)}[\mathbf{C}^{*}]^{-1}$$

and

$$\mathbf{B}^{\mathrm{th}(\alpha\beta\gamma)} = \mathbf{C}^{(\alpha\beta\gamma)}\mathbf{A}^{(\alpha\beta\gamma)}[\mathbf{C}^{*}]^{-1}\boldsymbol{\Gamma}^{*} + \mathbf{E}^{\mathrm{th}(\alpha\beta\gamma)}$$

The quantities $\mathbf{B}^{(\alpha\beta\gamma)}$ and $\mathbf{B}^{\mathrm{th}(\alpha\beta\gamma)}$ are referred to as the mechanical and thermal stress concentration tensors, respectively.

Consider a lattice block made of a metallic material that is subjected to an externally applied thermomechanical loading. Let us assume that yielding of material occupying subcell $(\alpha\beta\gamma)$ is determined from the von Mises condition:

$$\sigma_{\mathrm{eq}}^{(\alpha\beta\gamma)} = Y \tag{10}$$

In Eq. (10), the equivalent stress $\sigma_{\mathrm{eq}}^{(\alpha\beta\gamma)}$ is defined by

$$\sigma_{\mathrm{eq}}^{(\alpha\beta\gamma)} = \left[\frac{3}{2}\,\mathrm{dev}\,\bar{\boldsymbol{\sigma}}^{(\alpha\beta\gamma)}\,\mathrm{dev}\,\bar{\boldsymbol{\sigma}}^{(\alpha\beta\gamma)}\right]^{1/2}$$

where $\mathrm{dev}\,\bar{\boldsymbol{\sigma}}^{(\alpha\beta\gamma)}$ is the deviator of $\bar{\boldsymbol{\sigma}}^{(\alpha\beta\gamma)}$ and Y is the yield stress of the metallic material in simple tension. Accordingly, initial yielding of the lattice block is determined from the first subcell stress $\bar{\boldsymbol{\sigma}}^{(\alpha\beta\gamma)}$ which fulfills condition (10). Consequently, based on the present micromechanical theory, initial yield envelopes of a lattice block that is subjected to a given external loading $\bar{\boldsymbol{\sigma}}$ can be generated.

Traction-free lattice blocks, i.e., $\bar{\boldsymbol{\sigma}} = \mathbf{0}$, that are subjected to temperature variation do not yield. This is an expected result, since the metallic material that form the array can freely expand without developing any internal local stresses. Indeed, under these conditions the thermal stress concentration tensor $\mathbf{B}^{\mathrm{th}(\alpha\beta\gamma)} = \mathbf{0}$, so that $\bar{\boldsymbol{\sigma}}^{(\alpha\beta\gamma)} = \mathbf{0}$, see Eq. (9). Furthermore, the effective coefficients of thermal expansion of the lattice block are identical to the thermal expansion coefficients of its metallic material. Yielding at elevated temperature, on the other hand, can be obtained in a constrained lattice block by preventing it from expanding, namely by imposing that $\bar{\boldsymbol{\epsilon}} = \mathbf{0}$. In this situation, the local stresses $\bar{\boldsymbol{\sigma}}^{(\alpha\beta\gamma)}$ can be determined from Eq. (8) and initial yielding is determined by the first subcell which satisfies Eq. (10).

It is also possible to utilize Eq. (9) to predict damage thresholds when the lattice block is subjected to a specified isothermal external loading $\bar{\boldsymbol{\sigma}}$. To this end the damage criterion of Lemaitre and Chaboche (1990), which expresses the critical strain energy release rate by loss of stiffness, can be employed. It is given by

$$\left[\sigma_{\mathrm{eq}}\left(\frac{2}{3}(1+\nu) + 3(1-2\nu)(\sigma_h/\sigma_{\mathrm{eq}})^2\right)^{1/2}\right]^{(\alpha\beta\gamma)} = \sigma^* \tag{11}$$

where $\nu^{(\alpha\beta\gamma)}$ is the Poisson's ratio of the isotropic phase, $\sigma_h^{(\alpha\beta\gamma)}$ is the hydrostatic pressure and σ^* is a material parameter which specifies the stress at which damage occurs at a uniaxial state test. This expression, from which damage envelopes (that provide the onset of failure) can be generated, replaces the von Mises yield criterion (10).

3. Applications

The derived micromechanical equations are implemented herein to investigate various types of lattice blocks. These include elastic, elastoplastic, a lattice block that can provide negative Poisson's ratios, and two-phase lattice blocks that provide negative coefficients of thermal expansion (although the coefficients of thermal expansion of the materials are positive). For simplicity, the lengths, breadths and heights of all subcells were taken to be identical (cubic subcells). Changing these geometrical parameters results in variations of the material's volume fraction of the lattice block and the type of the effective anisotropy that it exhibits.

It should be mentioned that not every lattice block configuration is admissible. Some configurations are kinematically unstable and generate a singular matrix $\mathbf{K}$ in Eq. (3). This situation is well known in the analysis of large scale articulated structures as discussed, for example, by Armenakas (1988).

3.1. Elastic lattice blocks

Consider lattice blocks in which the material is assumed to behave as a perfectly elastic isotropic aluminum alloy at high temperature whose Young's modulus, Poisson's ratio and coefficient of thermal expansion are: 55 GPa, 0.3 and $23\times10^{-6}\,^{\circ}\mathrm{C}^{-1}$, respectively (it should be remembered that the effective coefficients of thermal expansion of the lattice block would have the same value of $23\times10^{-6}\,^{\circ}\mathrm{C}^{-1}$).

The lattice block whose unit cell is shown in Fig. 2 models an open cell material as discussed, for example, by Gibson and Ashby (1997). The solid material is distributed in linear members that form the cell edges (as opposed to the closed-cell case in which the solid material is distributed in little plates that form the faces of the cells). The unit cell consists of $N_\alpha = N_\beta = N_\gamma = 16$ cubic subcells and the resulting volume fraction of the material is: $v_f = 0.16$. It should be noted that the volume fraction of a lattice block is defined by the ratio between the total volume of filled subcells to the total volume of the filled and unfilled subcells. The specific configuration that is shown in Fig. 2 generates a composite whose effective behavior possesses a cubic symmetry (i.e., it is characterized by three independent material constants). The effective stiffness matrix $\mathbf{C}^*$ of this lattice block is given in Appendix A, Eq. (A.1).

The characteristic cell of Fig. 2 differs from a repeating unit cell by a proper adjustment of the size and shape of the cross section of the elements located at the surfaces. Therefore, in the sequel the term *repeating unit cell* will be continuously used.

Next, let us consider a lattice block composed of open cells the faces of which contain diagonal elements (to be referred to as "open cell-diagonal") as shown in Fig. 3. The repeating unit cell consists of $N_\alpha = N_\beta = N_\gamma = 30$ cubic subcells and the resulting volume fraction of the material is: $v_f = 0.19$. Due to the symmetry that exists in all three orthogonal directions, the resulting lattice block effectively exhibits a cubic symmetry. The micromechanically computed effective stiffness matrix $\mathbf{C}^*$ is given by Eq. (A.2) of Appendix A. It is readily seen that by ignoring the negligibly small elements in this matrix, cubic symmetry is actually obtained.

The next type of a lattice block has been considered by Zhou et al. (2004). These authors analyzed aluminum lattice blocks that consist of a pyramidal core structure and triangular planer truss faces. The unit cell of this lattice block is identical with that of Wallach and Gibson (2001). The repeating unit cell of Zhou et al. (2004) is shown in Fig. 4 and its micromechanical analysis has been carried out by its division into $N_\alpha = N_\beta = N_\gamma = 34$ cubic subcells, resulting in a material volume fraction of $v_f = 0.11$. The overall elastic

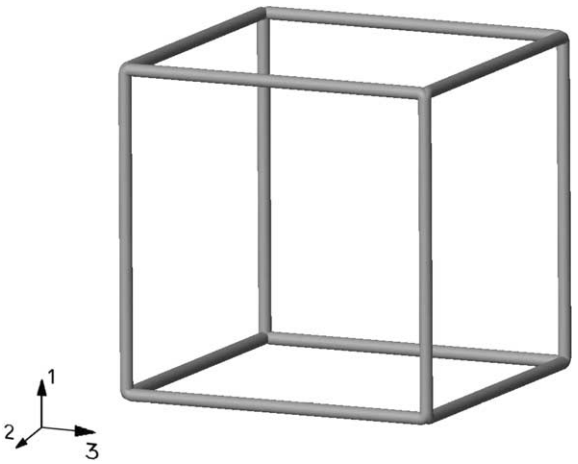

Fig. 2. The repeating unit cell with $N_\alpha = N_\beta = N_\gamma = 16$ subcells, that models the cellular solid with open cells. The material volume fraction is: $v_f = 0.16$.

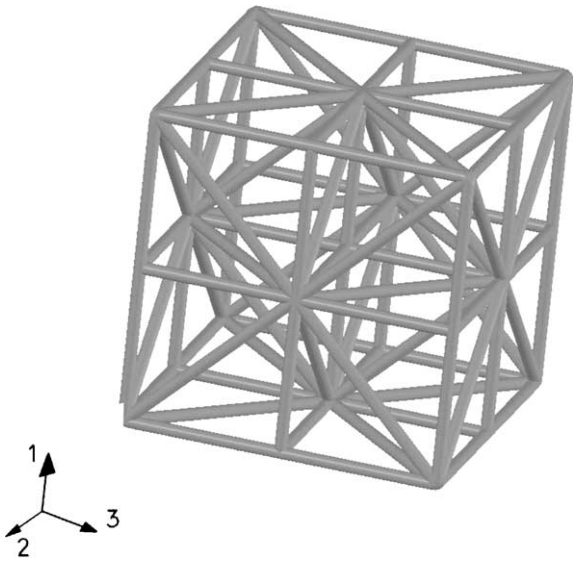

Fig. 3. The repeating unit cell of the lattice block which represents ''open cell-diagonal'' cellular solid. It is micromechanically analyzed with $N_\alpha = N_\beta = N_\gamma = 30$ subcells. The material volume fraction is: $v_f = 0.19$.

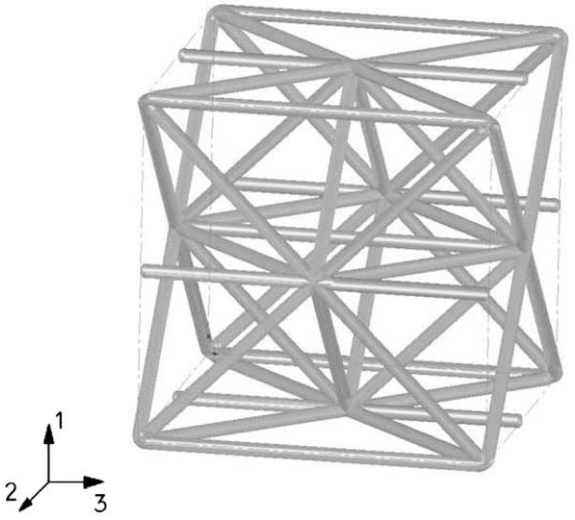

Fig. 4. The repeating unit cell of the lattice block of Zhou et al. (2004) is micromechanically analyzed with $N_\alpha = N_\beta = N_\gamma = 34$ subcells. The material volume fraction is: $v_f = 0.11$.

behavior of the present lattice block is represented by the micromechanically predicted effective stiffness matrix $\mathbf{C}^*$ that is given in Appendix A by Eq. (A.3). If the small value elements in this matrix are ignored, the resulting effective behavior that is represented by this matrix is orthotropic. It should be noted that the Young's modulus in the 3-direction ($E_3^* = 2180$ MPa) is about four time higher than the moduli in the other directions ($E_1^* = 522$ and $E_2^* = 520$ MPa).

The lattice block of Zhou et al. (2004) can be modified by replacing the horizontal layers by square and diagonal square arrays. The repeating unit cell of such a lattice block, referred to as ''square–diagonal'',

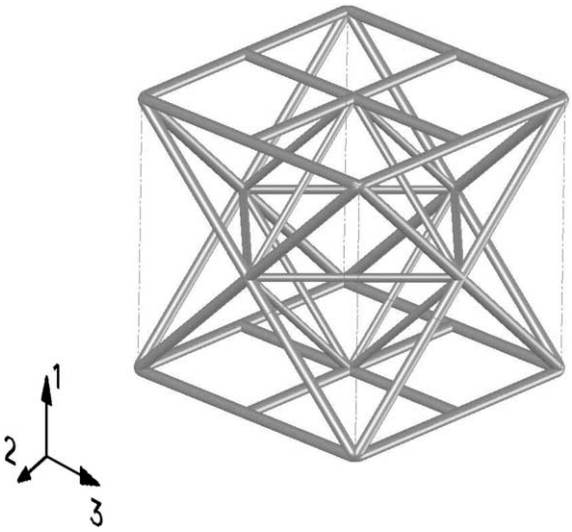

Fig. 5. The modified repeating unit cell of the lattice block of Zhou et al. (2004), referred to as ''square–diagonal'', is micromechanically analyzed with $N_\alpha = N_\beta = N_\gamma = 34$ subcells. The material volume fraction is: $v_f = 0.09$.

is presented in Fig. 5. This modification results in a material volume fraction of $v_f = 0.09$. The resulting effective stiffness matrix is given in Appendix A by Eq. (A.4). Again, if the small value elements of this matrix are ignored, the resulting stiffness resembles the behavior of a transversely isotropic material whose axis of symmetry is oriented in the x_1 direction. Nevertheless, this is not so because $c^*_{44} \neq (c^*_{22} + c^*_{23})/2$.

Consider next a lattice block whose repeating unit cell is shown in Fig. 6. It shows a material with two types of diagonal strips which is, following Deshpande et al. (2001), referred to as an ''octet'' configuration.

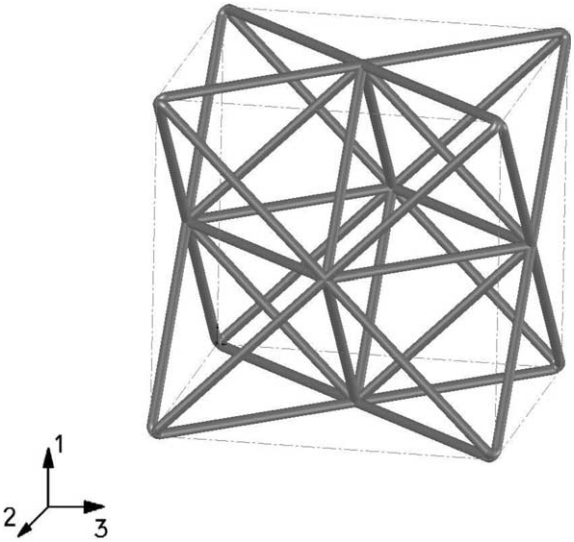

Fig. 6. The repeating unit cell of the octet lattice block is micromechanically analyzed with $N_\alpha = N_\beta = N_\gamma = 26$ subcells. The material volume fraction is: $v_f = 0.13$.

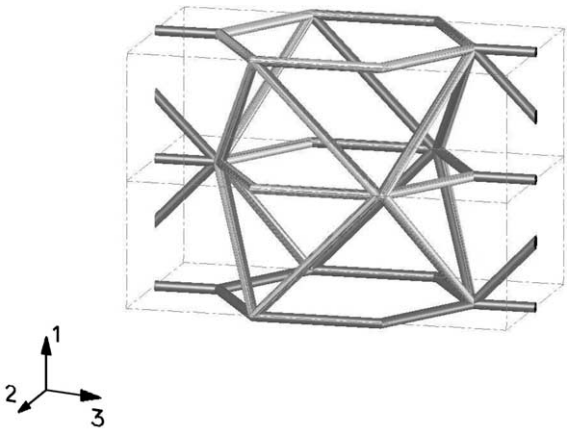

Fig. 7. The repeating unit cell of the lattice block with hexagonal arrays is micromechanically analyzed with $N_\alpha = 24$, $N_\beta = 18$ and $N_\gamma = 28$ subcells. The material volume fraction is: $v_f = 0.17$.

The resulting volume fraction of the material is: $v_f = 0.13$ and the effective stiffness matrix is given by Eq. (A.5). Here too, disregarding the small elements in the matrix shows that this lattice block behaves effectively as an orthotropic material.

Finally, let us consider a lattice block with a hexagonal array that forms the horizontal planes which are connected by spatial members. The arrangement of the latter, which has a tetragonal topology, has been discussed by Chiras et al. (2002). Its repeating unit cell appears in Fig. 7 which results in a material volume fraction of $v_f = 0.17$ and an effective stiffness matrix given by Eq. (A.6). It is readily seen that this lattice block is effectively characterized by an orthotropic material.

3.2. Elastoplastic lattice blocks

Elastoplastic behavior of lattice blocks is obtained when the material is loaded beyond its yield stress. In order to study the behavior under these circumstances, the previous aluminum alloy is assumed to behave as an elastic perfectly plastic material whose yield stress in simple tension is: $Y = 90$ MPa (and a yield strain of 0.16%). It should be mentioned that the present approach can handle elastoplastic strain-hardening materials. The perfectly plastic behavior assumption enables the examination of the global lattice block response in the plastic region by comparing it with the simple elastoplastic response of its parent solid material.

Our study of the response of elastoplastic lattice blocks starts with the simple configuration of open cells that was presented in Fig. 2. Fig. 8(a) exhibits the response of this lattice block to a uniaxial stress loading in the 1-direction (uniaxial loadings in directions 2 and 3 can be performed in the same manner providing identical responses). It is readily observed that contrary to the aluminum material, the composite response exhibit a slight strain hardening behavior. Fig. 8(b) shows the initial yield surface of the lattice block for a combined $\bar{\sigma}_{22} - \bar{\sigma}_{11}$ loading. The value of initial yielding at $\bar{\sigma}_{22} = 0$ obtained from this graph is $0.06Y$ which is consistent with the yielding point which is observed in Fig. 8(a). Fig. 8(c) shows the average stresses $\bar{\sigma}_{11} = \bar{\sigma}_{22} = \bar{\sigma}_{33}$ that are generated by the application of a temperature rise to 100 °C, while constraining the lattice block such that all average strains are kept equal to zero. According to Eq. (8), the critical temperature for the initiation of yielding at the present circumstances is 54 °C which is consistent with the value observed from Fig. 8(c). A careful check of the stress values generated by the temperature application (beyond 100 °C) reveals a slight hardening in the average stress–temperature response of the lattice block.

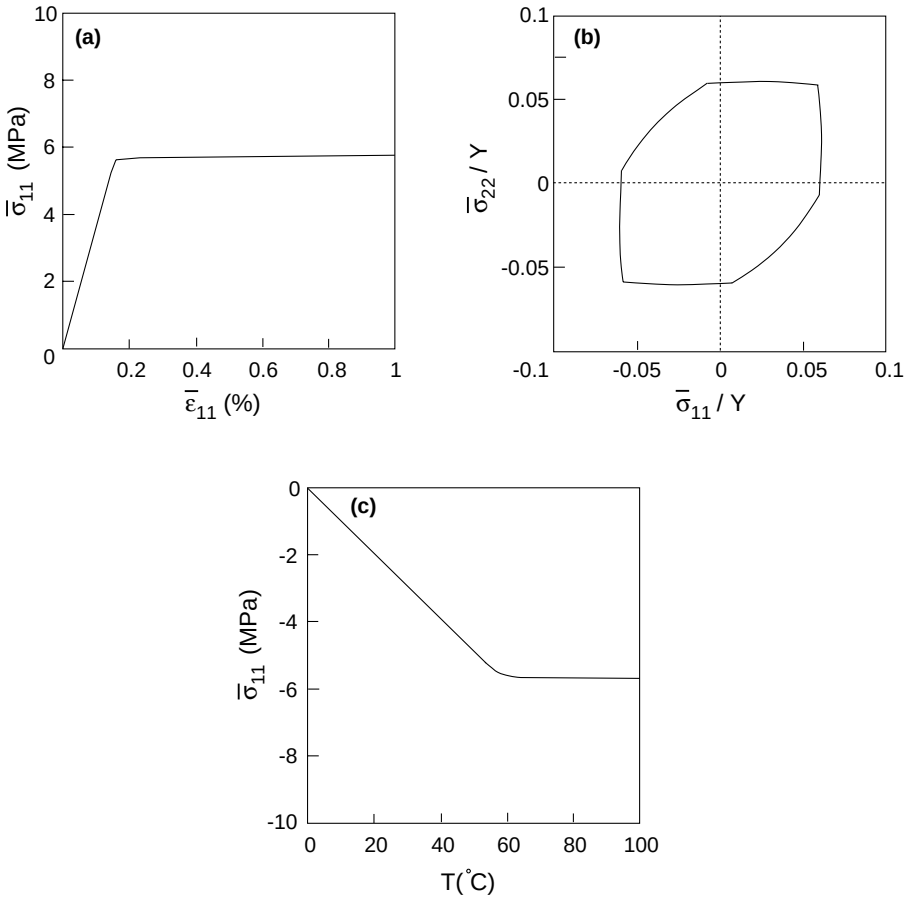

Fig. 8. (a) Uniaxial stress–strain response, (b) initial yield surface and (c) stress–temperature response of the elastoplastic lattice block whose repeating unit cell was shown in Fig. 2.

As will be apparent in the following, the inelastic behavior of lattice blocks may exhibit unexpected behavior. Hence, in order to carefully analyze this behavior let us proceed to a slightly more complicated configuration than the one shown in Fig. 2. To this end, consider the lattice block whose repeating unit cell is shown in Fig. 9 in which two crossing diagonal elements have been added to the top and bottom faces. Fig. 10(a) shows the uniaxial stress responses in the 1- and 2-directions. It is clearly observed that loading of the lattice block in the 1-direction exhibits a strain hardening over the entire range of applied strain. Loading in the 2-direction, on the other hand, can be performed up to a strain of $\bar{\epsilon}_{22} = 0.445\%$ (where $\bar{\sigma}_{22} = 8.7$ MPa), after which the stress–strain curve abruptly drops (namely, $\Delta\bar{\sigma}_{22}\ \Delta\bar{\epsilon}_{22} < 0$) and the computation process diverges indicating a structural instability. This peculiar behavior can be explained by observing the somewhat similar phenomena that takes place in nonlinear structures. As discussed by Majid (1972), load–deformation relations of nonlinear structures may exhibit at certain value of deformation a falling curve which indicates a failure of the elastic–plastic structure. The highest ordinate on this curve indicates the pre-mechanism state of failure. In the case of inelastic lattice block it appears that under a loading of certain direction and magnitude, the structure losses its stiffness and instability takes place namely, the load carrying capacity is lost. This situation is well exhibited by Fig. 10(a) which shows the

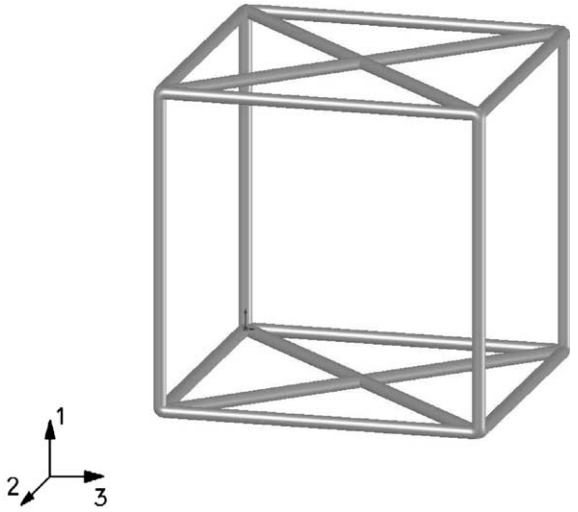

Fig. 9. The repeating unit cell of the lattice block of Fig. 2 in which diagonal strips have been added to the lower and upper surfaces. It is micromechanically analyzed with $N_\alpha = N_\beta = N_\gamma = 16$ subcells. The material volume fraction is: $v_f = 0.22$.

ability of the lattice block to sustain loading in the 1-direction, while a loss of stability occurs when it is loaded in the 2 or 3-direction. This inability of the lattice block to carry further loading resembles the limit load of plastic structures which is a property of the considered system. This property depends on the system's geometry and material behavior. The limit load of the lattice block is readily predicted by the micromechanical analysis which provides a design tool. Fig. 10(b) shows the initial yield surfaces of the present lattice block when loaded in the 1–2 and 2–3 directions. Finally, Fig. 10(c) shows the resulting stresses when the lattice block of Fig. 9 is subjected to a rising temperature, while keeping all its average stains equal to zero. Initial yielding due to temperature rise takes place, according to Eq. (8), at $T = 43\ ^\circ\mathrm{C}$. Beyond this temperature $\bar{\sigma}_{11}$ and $\bar{\sigma}_{22} = \bar{\sigma}_{33}$ reach the value of 4.5 and 8 MPa, respectively, after which an abrupt drop in these stresses take place with the divergence of the computational procedure indicating a structural instability similar to the mechanical loading case discussed before.

Let us consider the elastoplastic behavior of the "open cell-diagonal' lattice block with cubic symmetry whose repeating unit cell was shown on Fig. 3. Its elastoplastic response and initial yield surface are shown in Fig. 11. Here it is possible to load the lattice block up to a strain of about $\bar{\epsilon}_{11} = \bar{\epsilon}_{22} = \bar{\epsilon}_{33} = 0.25\%$, after which an abrupt drop and a divergence take place indicating an instability of the structure. The initial yield surface is smooth and resembles the yield surface of an isotropic material.

In Fig. 12, the uniaxial stress–strain curves and the initial yield surfaces are shown for the elastic-plastic lattice block of Zhou et al. (2004) the repeating unit cell of which has been presented in Fig. 4. It is readily seen that whereas the response in the 3-direction can be computed over the entire range of deformation, the elastoplastic response in the 2-direction exists up to $\bar{\epsilon}_{22} = 0.36\%$ after which the stability of the structure is lost. The uniaxial stress behavior of the lattice block in the 1-direction is quite similar to its behavior in the 2-direction and therefore it is not shown. This is also expressed by the observation that the initial yield surface $\bar{\sigma}_{33} - \bar{\sigma}_{11}$ (not shown in Fig. 12 (b)) is rather close to the $\bar{\sigma}_{33} - \bar{\sigma}_{22}$ surface. The induced average strains due to these uniaxial stress loadings in the 2- and 3-direction are shown in Fig. 13. The appreciable deviations from linearity due to the inelastic effects can be clearly observed. Let the lattice block of Zhou et al. (2004) be subjected to a temperature rise while keeping all average strains equal to zero. The initial yielding caused by this temperature elevation can be determined by employing Eq. (8) which provides the value of 51.7 °C. Fig. 14 exhibits the resulting average stresses induced by this temperature rise. It can be observed

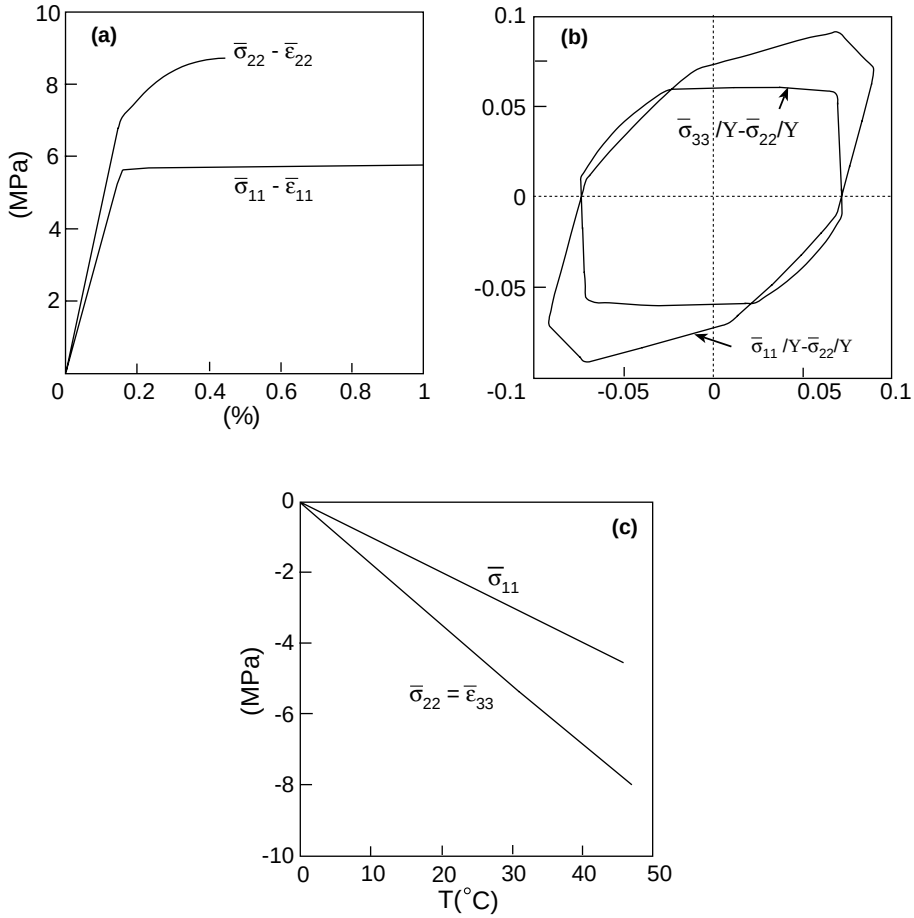

Fig. 10. (a) Uniaxial stress–strain responses in the 1- and 2-directions, (b) initial yield surfaces, and (c) stress–temperature response of the elastoplastic lattice block whose repeating unit cell was shown in Fig. 9.

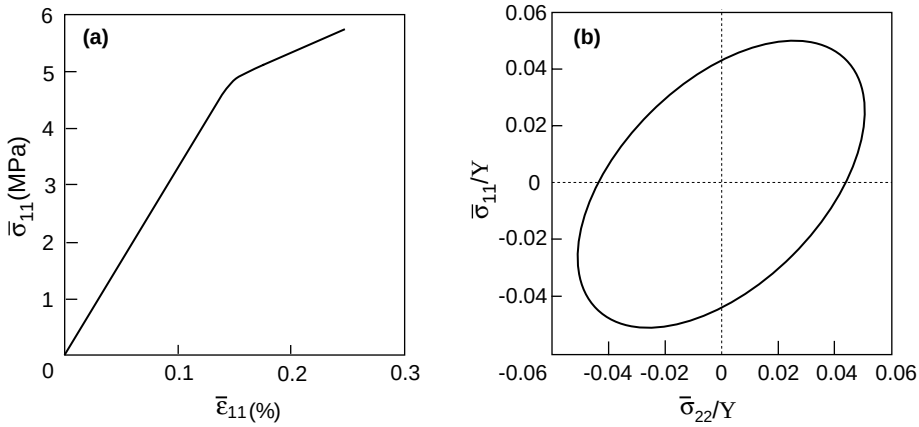

Fig. 11. (a) Uniaxial stress–strain responses in the 1, 2 and 3-directions, and (b) initial yield surface of the elastoplastic ''open cell-diagonal'' lattice block whose repeating unit was shown in Fig. 3.

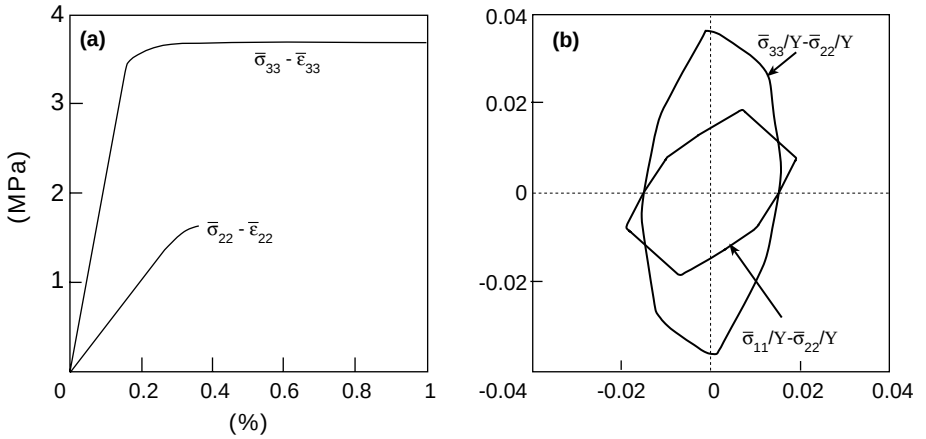

Fig. 12. (a) Uniaxial stress–strain response in the 2- and 3-directions, and (b) initial yield surfaces of the elastoplastic lattice block of Zhou et al. (2004) whose repeating unit was shown in Fig. 4.

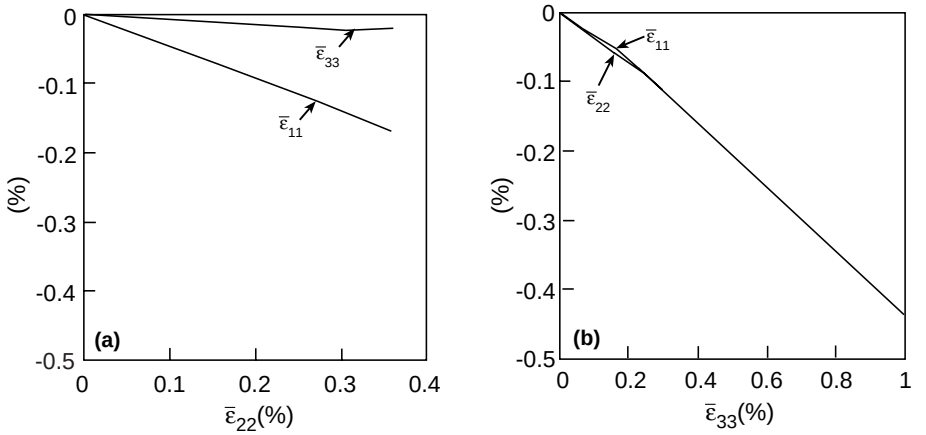

Fig. 13. (a) The resulting average strains induced by the uniaxial stress loading applied in the (a) 2-direction and (b) 3-direction of the elastoplastic lattice block of Zhou et al. (2004) whose repeating unit was shown in Fig. 4.

that slightly beyond the yield temperature instability of the lattice block occurs. Here too, the deviations from linearity can be well detected.

Finally, the initial yield surfaces of the lattice blocks whose repeating unit cells have been presented in Figs. 5–7 are shown in Fig. 15. In Fig. 15(a) the yield surface $\bar{\sigma}_{11} - \bar{\sigma}_{33}$ coincides with $\bar{\sigma}_{11} - \bar{\sigma}_{22}$ since the responses in 2- and 3-direction are identical. Due to the cubic symmetry of the lattice block of Fig. 6, Fig. 15(b) presents just one type of initial yield surface. This initial yield surface resembles the one presented by Deshpande et al. (2001) for the octet-truss lattice. The three initial yield surfaces that are shown in Fig. 15(c) reflect the fact that the lattice block of Fig. 7 is fully orthotropic.

Damage surfaces of lattice blocks can be generated by employing Eq. (11). For the types of lattice blocks considered in this investigation, results show that these surfaces are quite close to the corresponding initial yield surfaces.

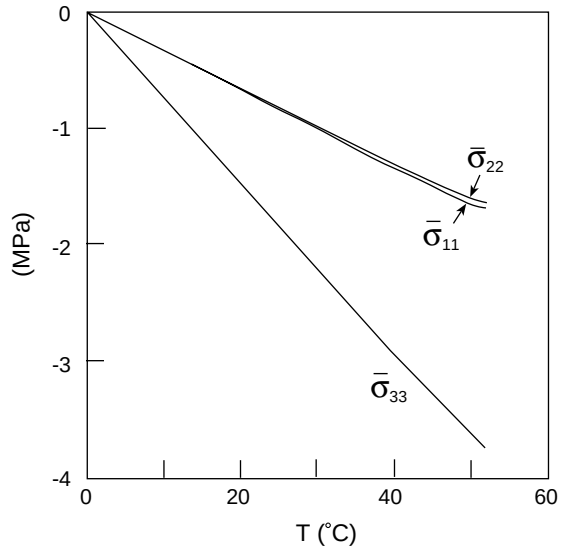

Fig. 14. Stress–temperature response of the elastoplastic lattice block of Zhou et al. (2004) whose repeating unit was shown in Fig. 4.

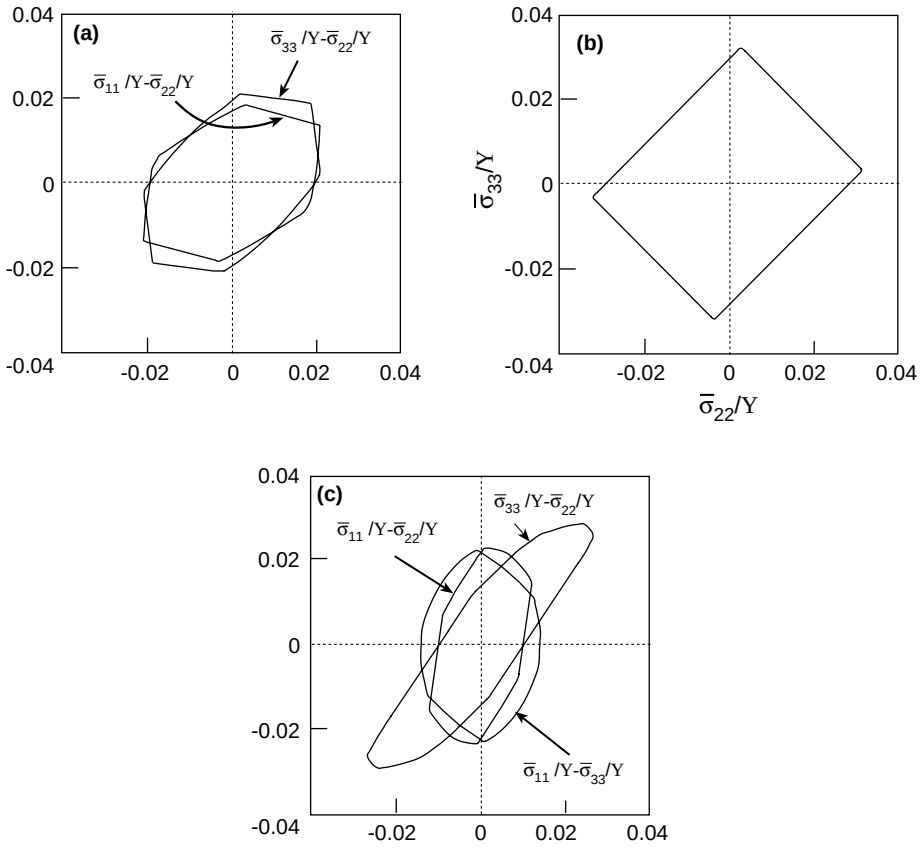

Fig. 15. Initial yield surfaces of: (a) square–diagonal (Fig. 5), (b) octet (Fig. 6), and (c) hexagonal (Fig. 7) lattice blocks.

3.3. Lattice blocks with negative Poisson's ratios

A three-dimensional analysis of a structure that is cable to generate negative Poisson's ratios has been presented by Choi and Lakes (1995). It is based on the analysis of spatial struts and curved beams. In the following, we employ the present micromechanical analysis to analyze and predict the negative Poisson's ratios of a lattice block the repeating unit cell of which is shown in Fig. 16. This lattice block is based on three re-entrant configurations in the three orthogonal directions. These configurations are capable to generate the requested negative Poisson's ratios. The micromechanical analysis has been employed by assuming that the lattice block material is identified by the elastic aluminum alloy whose properties have been given previously. The analysis predicts that the overall behavior of this lattice block is described by a cubic symmetry with three independent constants and its effective stiffness matrix $\mathbf{C}^*$ is shown by Eq. (A.7) of Appendix A. In particular, the following three effective Poisson's ratios can be readily established from $\mathbf{C}^*$:

$$v_{12}^* = v_{13}^* = v_{23}^* = -0.7$$

It should be noted that since the three effective Young's moduli E_1^*, E_2^* and E_3^* are equal ($E_1^* = E_2^* = E_3^* = 193.5$ MPa), the general requirements, Jones (1975), that

$$|v_{ij}^*| < \sqrt{\frac{E_i^*}{E_j^*}}$$

are satisfied.

3.4. Two-phase lattice blocks with negative coefficients of thermal expansion

As previously mentioned, the effective coefficients of thermal expansion of lattice blocks consisting of a single parent material are identical to those of the material itself. It is possible however to construct lattice

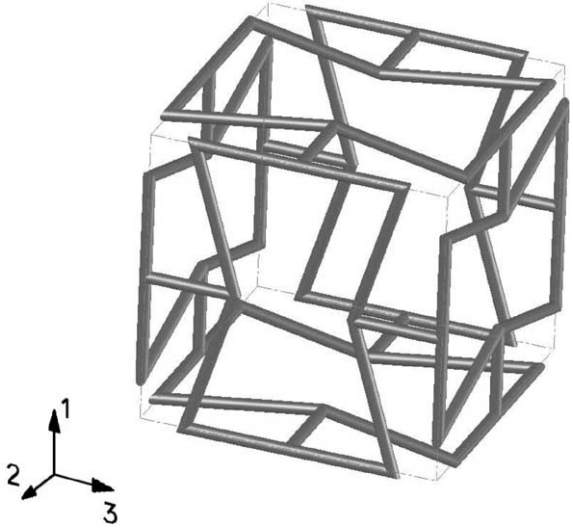

Fig. 16. The repeating unit cell of a lattice block which consists of three re-entrant configurations in the three orthogonal directions that generate negative Poisson's ratios. The repeating unit cell is micromechanically analyzed with $N_\alpha = N_\beta = N_\gamma = 30$ subcells. The material volume fraction is: $v_f = 0.09$.

blocks that consist of two distinct materials such that the effective coefficients of thermal expansion are negative although the coefficients of thermal expansion of the two parent materials are positive. In the two-dimensional case, Kalamkarov and Kolpakov (1997) proposed a framework consisting of materials whose thermal expansion coefficients are positive, that can generate negative coefficients of thermal expansion.

Here, we propose two configurations of two-phase lattice blocks, whose repeating unit cell are shown in Fig. 17, that can generate negative effective coefficients of thermal expansion. The Young's moduli, Poisson's ratios and coefficients of thermal expansion of phase 1 and 2 are given in Table 1. The micromechanical analysis of the repeating unit of Fig. 17(a) predicts that the effective coefficients of thermal expansion in the 1- and 2-directions are negative and given, respectively, by: -1.9×10^{-6} and $-1.1\times10^{-6}\,^{\circ}\mathrm{C}^{-1}$. The analysis of Fig. 17(b), on the other hand, predicts a negative effective coefficient of thermal expansion in the 1-direction of $-1.8\times10^{-6}\,^{\circ}\mathrm{C}^{-1}$ whereas in the 2- and 3-direction the effective coefficients are positive.

The negative coefficient of thermal expansion a lattice block can be best explained by referring to Fig. 17(b). This configuration consists of two pyramids with a common plane. The common plane contains four

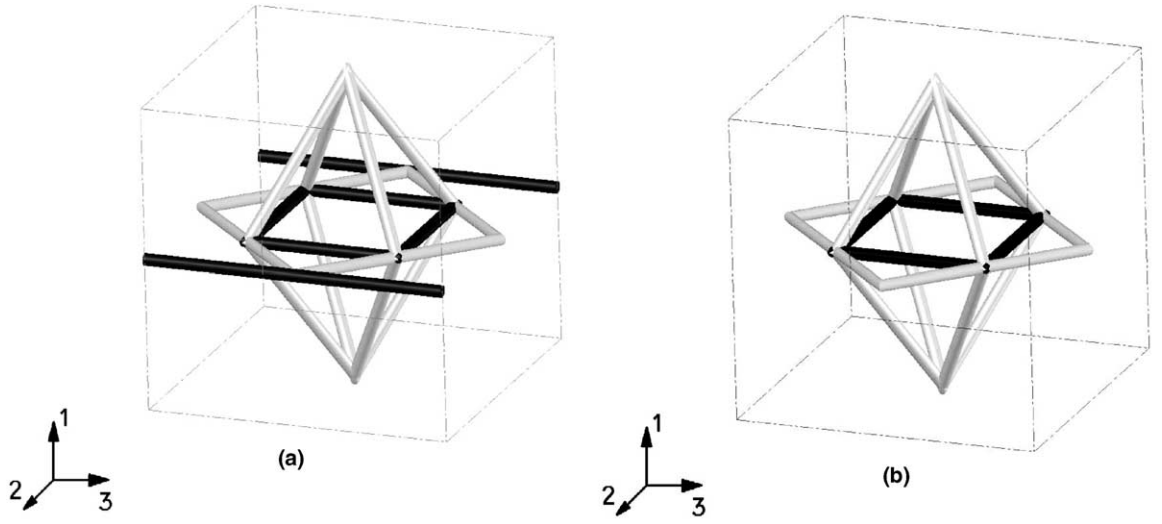

Fig. 17. The repeating unit cell of two-phase lattice blocks that can generate negative effective coefficients of thermal expansion. The repeating unit cell is micromechanically analyzed with $N_\alpha = 25$, $N_\beta = N_\gamma = 24$ subcells. Phase 2 is depicted by the darker regions. (a) A configuration that generates negative coefficients of thermal expansions in the 1- and 2-directions. The volume fractions of phase 1 and 2 are 0.076 and 0.032, respectively. (b) A configuration that generates a negative coefficient of thermal expansion in the 1-direction. The volume fractions of phase 1 and 2 are 0.076 and 0.019, respectively.

Table 1
Material constants of the two parent phases of the lattice blocks whose effective coefficients of thermal expansion are negative

	Young's modulus (GPa)	Poisson's ratio	Coefficient of thermal expansion ($10^{-6}\,^{\circ}\mathrm{C}^{-1}$)
Material 1	1	0.45	1
Material 2	10	0.2	10

members with high coefficient of thermal expansion. By applying a temperature increase, the common plane expands yielding a "mechanical" contraction normal to the plane. This contraction overcomes the expansion due to the temperature increase thus yielding a negative coefficient of thermal expansion of the lattice block in the 1-direction.

To conclude this section, it should be noted that in the present investigation we focus on the relation between the microstructure and global behavior of the lattice block. On the other hand, it is obvious that the volume fraction does not qualitatively affect the overall characteristics of the lattice block. Hence the drawn conclusions reported above are valid irrespective of the various values of the volume fraction used in this paper.

4. Conclusions

Lattice blocks are periodic structures in which their repeating unit cells are usually analyzed by considering the beams and columns that form these cells. In the present paper an alternative approach for the analysis of lattice blocks is presented. According to this continuum mechanics-based approach, the lattice blocks are analyzed by implementing a micromechanical procedure (which has been developed for the prediction of the behavior of multi-phase composites) whose veracity has been previously established in several circumstances. In order to save computer memory and execution time, a special strategy has been implemented according to which the micromechanical procedure is applied only to filled regions of the repeating unit cell that forms the lattice block. The global elastic and elastoplastic behaviors of several types lattice blocks have been shown.

A particular advantage of the use of a micromechanical approach in the investigation of the behavior of a composite material (in our case a multi-phase lattice block) is expressed by the fact that the analysis relies on the properties of the individual constituents, which are usually isotropic, and their relative volume ratios. Hence one does not need to consider anisotropic yield or damage criteria nor anisotropic inelastic flaw rules in order to investigate the global behavior of the composite. The global anisotropic behavior is merely a byproduct of the micromechanical analysis. The present approach provides a quantitative vehicle which is capable of predicting the elastic and inelastic properties of a lattice block. The analysis can be used by a material designer in order to compare the performance of various configurations with respect to a specific required property (e.g. the effective Young's modulus, yield point, type of anisotropy, etc...).

Extension of the present micromechanical approach to investigate the buckling and the large deformation of lattice blocks are topics for a future research.

Acknowledgement

The first author gratefully acknowledges the support of the Diane and Arthur Belfer chair of Mechanics and Biomechanics. Also special thanks go to Mr. Z. Genosar for the generation of the lattice block drawings.

Appendix A

The effective stiffness matrix of the lattice block that represents the behavior of the open cell material of Fig. 2 is given by

$$\mathbf{C}^*(\mathrm{MPa}) = \begin{bmatrix} 3660 & 286 & 286 & 0 & 0 & 0 \\ & 3660 & 286 & 0 & 0 & 0 \\ & & 3660 & 0 & 0 & 0 \\ & & & 180 & 0 & 0 \\ & & & & 180 & 0 \\ \text{sym.} & & & & & 180 \end{bmatrix} \tag{A.1}$$

The effective stiffness matrix of the lattice block that represents the behavior of the open cell-diagonal configuration of Fig. 3 is given by

$$\mathbf{C}^*(\mathrm{MPa}) = \begin{bmatrix} 3570 & 753 & 753 & 0.05 & -0.13 & -0.13 \\ & 3570 & 753 & 0.13 & -0.05 & -0.13 \\ & & 3570 & 0.13 & -0.13 & -0.05 \\ & & & 607 & 0.11 & 0.11 \\ & & & & 607 & -0.11 \\ \text{sym.} & & & & & 607 \end{bmatrix} \tag{A.2}$$

The effective stiffness matrix of the lattice block that is discussed by Zhou et al. (2004) and shown in Fig. 4 is given by

$$\mathbf{C}^*(\mathrm{MPa}) = \begin{bmatrix} 722 & 360 & 389 & 0.06 & -0.21 & 0.1 \\ & 713 & 369 & 0.27 & 0.01 & 0.1 \\ & & 2450 & 0.25 & -0.09 & -0.02 \\ & & & 349 & 0.04 & 0.06 \\ & & & & 353 & -0.06 \\ \text{sym.} & & & & & 340 \end{bmatrix} \tag{A.3}$$

The effective stiffness matrix of the "square–diagonal" lattice block of whose repeating unit cell is shown in Fig. 5.

$$\mathbf{C}^*(\mathrm{MPa}) = \begin{bmatrix} 722 & 369 & 369 & -0.14 & -0.12 & 0.75 \\ & 1430 & 254 & -0.41 & -0.17 & 0.51 \\ & & 1430 & -0.02 & 0.02 & 0.10 \\ & & & 186 & -0.23 & 0.09 \\ & & & & 340 & -0.16 \\ \text{sym.} & & & & & 340 \end{bmatrix} \tag{A.4}$$

The effective stiffness matrix of the octet lattice block whose repeating unit cell is shown in Fig. 6.

$$\mathbf{C}^*(\mathrm{MPa}) = \begin{bmatrix} 1320 & 681 & 681 & 0 & 0 & 0 \\ & 1320 & 690 & -0.92 & 0.15 & 0.15 \\ & & 1320 & -0.92 & 0.15 & 0.15 \\ & & & 641 & -0.07 & -0.07 \\ & & & & 639 & 0.07 \\ \text{sym.} & & & & & 639 \end{bmatrix} \tag{A.5}$$

The effective stiffness matrix of the lattice block with hexagonal strips whose repeating unit cell is shown in Fig. 7.

$$\mathbf{C}^*(\mathrm{MPa}) = \begin{bmatrix} 948 & 506 & 533 & 0 & 0 & 0 \\ & 1320 & 1240 & 0 & 0 & 0 \\ & & 1490 & 0 & 0 & 0 \\ & & & 242 & 0 & 0 \\ & & & & 373 & 0 \\ \text{sym.} & & & & & 294 \end{bmatrix} \tag{A.6}$$

The effective stiffness matrix of the lattice block with orthogonal re-entrant configurations whose repeating unit cell is shown in Fig. 16.

$$\mathbf{C}^*(\mathrm{MPa}) = \begin{bmatrix} 452 & -186 & -186 & 0 & 0 & 0 \\ & 452 & -186 & 0 & 0 & 0 \\ & & 452 & 0 & 0 & 0 \\ & & & 2.1 & 0 & 0 \\ & & & & 2.1 & 0 \\ \text{sym.} & & & & & 2.1 \end{bmatrix} \tag{A.7}$$

References

Aboudi, J., 2001. Micromechanical analysis of fully coupled electro-magneto-thermo-elastic multiphase composites. Smart Mater. Struct. 10, 867–877.

Aboudi, J., 2004. The generalized method of cells and high-fidelity generalized method of cells micromechanical models—a review. Mech. Adv. Mater. Struct. 11, 329–366.

Aboudi, J., Pindera, M.J., Arnold, S.M., 2001. Linear thermoelastic higher-order theory for periodic multiphase materials. J. Appl. Mech. 68, 697–707.

Aboudi, J., Pindera, M.J., Arnold, S.M., 2003. Higher-order theory for periodic multiphase materials with inelastic phases. Int. J. Plasticity 19, 805–847.

Almgren, R.F., 1985. An isotropic three-dimensional structure with negative Poisson's ratio = −1. J. Elasticity 15, 427–430.

Armenakas, A.E., 1988. Classical Structural Analysis. McGraw Hill, New York.

Bednarcyk, B.A., Arnold, S.M., 2002. MAC/GMC 4.0 User's Manual. NASA/TM-2002-212077, 2002.

Bednarcyk, B.A., Arnold, S.M., Aboudi, J., Pindera, M.-J., 2004. Local field effects in titanium matrix composites subject to fiber-matrix debonding. Int. J. Plasticity 20, 1707–1737.

Chiras, S., Mumm, D.R., Evans, A.G., Wicks, N., Hutchinson, J.W., Dharmasena, K., Wadley, H.N.G., Fichter, S., 2002. The structural performance of near-optimized truss core panels. Int. J. Solids Struct. 39, 4093–4115.

Choi, J.B., Lakes, R.S., 1995. Nonlinear analysis of the Poisson's ratio of negative Poisson's ratio foams. J. Compos. Mat. 29, 113–128.

Deshpande, N.A., Fleck, N.A., Ashby, M.F., 2001. Effective properties of the octet-truss lattice material. J. Mech. Phys. Solids 49, 1747–1769.

Evans, A.G., Hutchinson, J.W., Fleck, N.A., Ashby, M.F., Wadley, H.N.G., 2001. The topological design of multifunctional cellular metals. Prog. Mater. Sci. 46, 309–327.

Gibson, L.J., Ashby, M.F., 1997. Cellular Solids. Cambridge University Press, Cambridge, UK.

Hutchinson, R.G., Wicks, N., Evans, A.G., Fleck, N.A., Hutchinson, J.W., 2003. Kagome plate structures for actuation. Int. J. Solids Struct. 40, 6969–6980.

Jones, R.M., 1975. Mechanics of Composite Materials. Scripta Book Company, Washington, DC.

Kalamkarov, A.L., Kolpakov, A.G., 1997. Analysis, Design and Optimization of Composite Structures. John Wiley & Sons, New York.

Lakes, R., 1987. Foam structures with a negative Poisson's ratio. Science 235, 1038–1040.

Lemaitre, J., Chaboche, J.L., 1990. Mechanics of Solid Materials. Cambridge University Press, Cambridge.

Majid, K.I., 1972. Non-linear Structures. Butterworths, London.
Wallach, J.C., Gibson, L.J., 2001. Mechanical behavior of a three-dimensional truss material. Int. J. Solids Struct. 38, 7181–7196.
Wang, A.-J., McDowell, D.L., 2005. Yield surfaces of various periodic metal honeycombs at intermediate relative density. Int. J. Plasticity 21, 285–320.
Wicks, N., Hutchinson, J.W., 2001. Optimal truss plates. Int. J. Solids Struct. 38, 5165–5183.
Wicks, N., Hutchinson, J.W., 2004. Performance of sandwich plates with truss cores. Mech. Mater. 36, 739–751.
Zhou, J., Shrotriya, P., Soboyejo, W.O., 2004. On the deformation of aluminum lattice block structures: from struts to structures. Mech. Mater. 36, 723–737.